

# Parallel Wavelength-Division-Multiplexed Signal Transmission and Dispersion Compensation Enabled by Soliton Microcombs and Microrings

Liangjun Lu (✉ [luliangjun@sjtu.edu.cn](mailto:luliangjun@sjtu.edu.cn))

Shanghai Jiao Tong University

Yuanbin Liu

Shanghai Jiao Tong University

Hongyi Zhang

Shanghai Jiao Tong University

Jiacheng Liu

Shanghai Jiao Tong University

Jiangbing Du

Shanghai Jiao Tong University <https://orcid.org/0000-0002-6333-824X>

Yu Li

Shanghai Jiao Tong University

Zuyuan He

Shanghai Jiao Tong University

Jianping Chen

Shanghai Jiaotong University

Linjie Zhou

Shanghai Jiao Tong University <https://orcid.org/0000-0002-2792-2959>

Andrew Poon

Hong Kong University of Science and Technology <https://orcid.org/0000-0002-5222-8184>

---

## Article

## Keywords:

**Posted Date:** September 18th, 2023

**DOI:** <https://doi.org/10.21203/rs.3.rs-3282850/v1>

**License:**   This work is licensed under a Creative Commons Attribution 4.0 International License.

[Read Full License](#)

**Additional Declarations:** There is **NO** Competing Interest.

---

# Parallel Wavelength-Division-Multiplexed Signal Transmission and Dispersion Compensation Enabled by Soliton Microcombs and Microrings

Yuanbin Liu<sup>1,4</sup>, Hongyi Zhang<sup>1,4</sup>, Jiacheng Liu<sup>1,4</sup>, Liangjun Lu<sup>1,2,\*</sup>, Jiangbing Du<sup>1,\*</sup>, Yu Li<sup>1,2</sup>, Zuyuan He<sup>1</sup>, Jianping Chen<sup>1,2</sup>, Linjie Zhou<sup>1,2</sup>, and Andrew W. Poon<sup>3</sup>

<sup>1</sup>State Key Laboratory of Advanced Optical Communication Systems and Networks, Shanghai Key Lab of Navigation and Location Services, Department of Electronic Engineering, Shanghai Jiao Tong University, Shanghai 200240, China

<sup>2</sup>SJTU-Pinghu Institute of Intelligent Optoelectronics, Pinghu 314200, China

<sup>3</sup>Photonic Device Laboratory, Department of Electronic and Computer Engineering, The Hong Kong University of Science and Technology, Clear Water Bay, Hong Kong

\*Corresponding authors' e-mail address: [luliangjun@sjtu.edu.cn](mailto:luliangjun@sjtu.edu.cn), [dujiangbing@sjtu.edu.cn](mailto:dujiangbing@sjtu.edu.cn)

<sup>4</sup>These authors contributed equally to this work.

## Abstract

The proliferation of computation-intensive technologies has led to a significant rise in the number of datacenters, posing challenges for high-speed and power-efficient datacenter interconnects (DCIs). Although inter-DCIs based on intensity modulation and direct detection (IM-DD) along with wavelength-division multiplexing (WDM) technologies exhibit cost-effective, power-efficient, and large-capacity properties, the requirement of multiple laser sources leads to high costs and limited scalability. Moreover, careful considerations must be given to the chromatic dispersion in the C-band as it restricts the transmission length of the optical signals. Electronic and optical approaches based on digital signal processing algorithms or dispersion-compensating fibers suffer from either a high power consumption or a lack of full reconfigurability. In this study, we present an original scalable on-chip parallel IM-DD data transmission system enabled by a single-soliton Kerr microcomb and a reconfigurable microring resonator (MRR)-based dispersion compensator. The highly compact MRR-based Kerr microcomb and dispersion compensator are intrinsically compatible with the parallel processing nature of the WDM link. Besides, the reconfigurability of the dispersion compensator shows the validation for various data-rate transmissions over multiple single-mode fiber lengths of up to 40 km, with a power consumption of below 160 mW, regardless of the modulation format or of the number of transmission channels utilized. Through our experimental validation, we demonstrate an aggregate bit rate of 1.68 Tbit/s over a 20-km-long single-mode fiber using 15 independent wavelength channels spaced at 100 GHz. Our approach holds significant promise for achieving data communications at a scale exceeding 10 terabits, making it highly valuable for future hyper-scale DCIs.

## Introduction

According to the International Data Corporation (IDC), the exponential growth of digital data

generation is projected to reach 175 zettabytes by 2025<sup>1</sup> due to the surgent growth of computation-intensive technologies such as artificial intelligence, Internet of Things (IoT), and autonomous vehicles. The total data capacity grows 80 times from 640 GHz in 2010 to 51.2 THz in 2022 for data switching in datacenter interconnects (DCIs) while the total power consumption grows 22 times<sup>2</sup>. As a result, there is a critical need for energy-efficient and cost-effective DCIs that can accommodate a substantial capacity. For short-reach DCIs spanning distances of less than 40 km, the utilization of intensity modulation and direct detection (IM-DD) has emerged as a practical and preferred solution<sup>3-5</sup>. This choice is motivated by the inherent advantages IM-DD offers, including cost-effectiveness, a low power consumption, and a compact physical footprint. Due to the lower data rate of the IM-DD system for a single wavelength channel than the coherent scheme, wavelength-division multiplexing (WDM) technology is commonly employed to economically enhance the data capacity. However, multiple laser sources are required to provide multiple operation wavelengths in the WDM systems, which leads to a higher cost. Moreover, in IM-DD systems operating within the C-band, the transmission distance is primarily limited by chromatic dispersion (CD), necessitating effective mitigation strategies<sup>6-8</sup>. The CD-induced frequency-selective fading (FSF) significantly impacts transmission performance<sup>9, 10</sup>. To address the dispersion effect, various electronic and optical approaches have been employed, such as digital signal processing (DSP)<sup>11-13</sup> and dispersion-compensating fibers (DCFs). However, these methods are burdened with limitations, particularly in terms of a high energy consumption and associated costs<sup>14</sup>.

Chip-scaled soliton microcombs, known for their wide spectral range, low noise, and high repetition rate, have emerged as a promising light source for WDM applications<sup>15-24</sup>. Recent advancements have demonstrated massively parallel data transmission using various types of microcomb sources, including bright single-solitons<sup>25</sup>, perfect soliton crystals<sup>26</sup>, and dark solitons<sup>27</sup>. For example, the utilization of two interleaved single-soliton microcombs in a silicon nitride ( $\text{Si}_3\text{N}_4$ ) microresonator enabled coherent data transmission with 179 carriers in the C- and L-bands, achieving a total bit rate of 55 Tb/s<sup>25</sup>. Similarly, the soliton crystal with defects, generated in a doped silica glass microresonator, facilitated a line rate of 40.1 Tb/s and a spectral efficiency of 10.2 b/s/Hz<sup>26</sup>. However, it is critical to note that the majority of WDM transmission systems utilizing soliton microcombs rely on expensive coherent schemes, necessitating costly transmitters and receivers<sup>25-30</sup>. Recently, massively parallel optical interconnects based on a  $\text{Si}_3\text{N}_4$  Kerr dark soliton comb source and a silicon microdisk modulator array with a data rate of 512 Gb/s for IM-DD transmission have been demonstrated<sup>31</sup>. In addition, a parallel optical data link driven by an AlGaAs Kerr microcomb has achieved a data rate of 2 Tbit/s in the IM-DD system<sup>32</sup>. However, we note that these transmission techniques are limited in term of transmission lengths and are primarily suitable for intra-DCI applications.

In recent years, the adoption of silicon photonics facilitated the integration of various silicon-based photonic devices, including chirped Bragg gratings<sup>33-37</sup>, Mach-Zehnder interferometers (MZIs)<sup>38, 39</sup>, and microring resonators (MRRs)<sup>40-46</sup>, to effectively mitigate the impact of CD in single-mode fibers (SMFs). These integrated devices offer several advantages, including a compact form factor, cost efficiency, a low power consumption, and a high reconfigurability. While imbalanced MZIs and MRRs demonstrate desirable characteristics for parallel signal processing due to their periodic spectral properties, their potential in WDM systems is currently limited. As a result, existing studies have reported only a modest maximum data transmission rate of 224 Gbit/s<sup>44</sup>.

In this paper, we present an original approach for short-reach inter-DCIs based on an IM-DD

optical communications architecture. Our proposed system leverages a single-soliton microcomb source generated by a  $\text{Si}_3\text{N}_4$  MRR as an WDM light source. Furthermore, we introduce a fully reconfigurable optical dispersion compensator based on cascaded silicon MRRs for parallel dispersion compensation. This WDM-assisted IM-DD scheme offers numerous advantages, including a high scalability, compactness, energy efficiency, and cost-effectiveness. To evaluate the performance of our proposed system, we conducted experiments demonstrating parallel signal transmission using up to 15 wavelength channels within the C-band. By employing pulse-amplitude four-level (PAM4) modulation signals at a rate of 80 Gbit/s, we achieved an aggregate data rate of 1.2 Tbit/s. Additionally, by employing discrete multi-tone (DMT) modulation signals at a rate of 112 Gbit/s, we achieved an aggregate data rate of 1.68 Tbit/s. These transmission rates were achieved over a 20-km-length SMF. Importantly, we assessed the power consumption of the dispersion compensator to be consistently below 160 mW, regardless of the modulation format or the number of transmission channels utilized. By aligning the free spectral range (FSR) of the Kerr MRR and the dispersion compensator and further increasing the number of wavelength channels, we expect the transmission capacity to exceed 10 Tbit/s. This capability holds significant promise for meeting the demands of future hyperscale DCIs.

## Results

### Parallel IM-DD data transmission and dispersion compensation architecture

Figure 1a shows the schematics of the integrated parallel data communications system for IM-DD applications. At the transmitter, a bright single-soliton microcomb with a smooth spectrum, which is generated by a  $\text{Si}_3\text{N}_4$  microresonator, is utilized as the multi-wavelength laser source with evenly distributed and low-noise frequency tones. The comb source is then demultiplexed, independently encoded with electrical data, and multiplexed by silicon microring modulator (MRM) arrays working at several individual wavelength channels. The modulated data are transmitted through an SMF before being sent to the receiver. The MRMs have the advantages of a compact size and of a high modulation bandwidth, which have been demonstrated with a modulation bandwidth of 110 GHz<sup>47</sup>. To increase the channels and to reduce the crosstalk, de-/multiplexers based on MRRs<sup>48-50</sup>, asymmetric MZIs<sup>51, 52</sup>, and MRR-coupled MZIs<sup>53, 54</sup> can be inserted before and after the silicon MRR modulator arrays. At the receiver end, we employ a silicon-based dispersion compensator utilizing cascaded MRRs to simultaneously compensate for the dispersion induced by SMF transmission across all the wavelength channels. The FSR of the cascaded MRRs is designed to match the wavelength spacing of the frequency combs. Moreover, the resonant wavelengths and the coupling coefficients of each MRR can be independently adjusted, offering a fully reconfigurable configuration that caters to various transmission ranges and operation bandwidths. Following the compensation process, the signal is then separated into distinct wavelength channels with MRR-based demultiplexers for photodetection. This comprehensive system enables parallel data transmission and dispersion compensation through the integration of photonic devices, featuring a simple arrangement and remarkable scalability. Consequently, our approach holds great promise for the development of fully integrated photonic circuits, especially for high-capacity inter-DCIs.

In this proof-of-concept study, we used a  $\text{Si}_3\text{N}_4$  microresonator with a bending radius of 232  $\mu\text{m}$  and an average quality (Q) factor of  $7 \times 10^5$  for single-soliton generation. Figure 1b shows the microscope image of the fabricated  $\text{Si}_3\text{N}_4$  microresonator. The waveguide cross-section is  $1800 \times 800 \text{ nm}^2$  and the measured second-order group-velocity dispersion ( $D_2/2\pi$ ) is 601.2 kHz<sup>55</sup>.

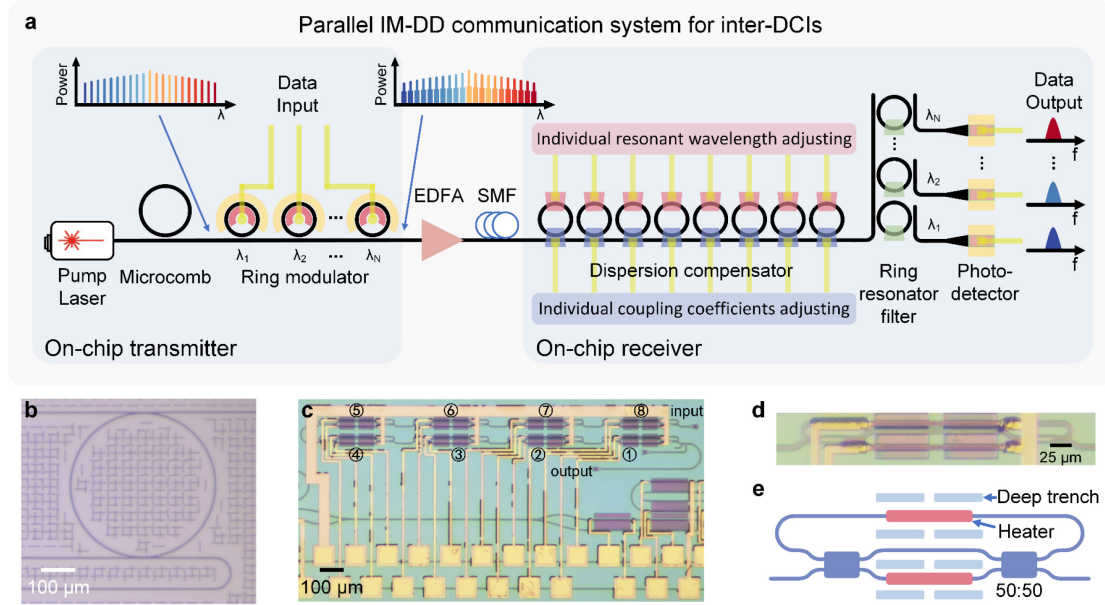


**Fig 1. Chip-based parallel data communication architecture for short-reach inter-DCIs.** **a** Schematics of the data transmission system. At the transmitter, a multi-wavelength laser source with an equal channel spacing is generated by a Si<sub>3</sub>N<sub>4</sub> Kerr MRR, and then individually intensity-modulated by integrated MRR modulator arrays. After that, the modulated multi-wavelength optical signal transmits through an SMF. At the receiver side, the parallel WDM signals are first processed by a cascaded-MRRs-based optical signal processor for dispersion compensation, and then demultiplexed by MRR filter arrays and received by photodetectors separately. **b** Microscope image of the Si<sub>3</sub>N<sub>4</sub> micro-resonator for single-soliton generation. **c** Microscope image of the silicon-MRRs-based dispersion compensator. The numbers label the self-defined sequence of each ring, and the input and output ports are labeled. **d** Enlarged view of a silicon MRR in the dispersion compensator. **e** Schematics of the silicon MRR.

The FSR is about 97.7 GHz. We utilized a program-controlled scheme based on thermal auxiliary compensation to generate and to stabilize the microcomb in the whole experiments<sup>56</sup>. See Supplementary Note 1 for the detailed program-controlled scheme for the single-soliton generation and stabilization. At the receiver side, the fully reconfigurable silicon dispersion compensator comprises 8 identical MRRs. Figure 1c shows the microscope image of the device. Figures 1d and 1e demonstrate the enlarged microscope image and the schematics of one MRR, respectively. The FSR of these MRRs is around 99.5 GHz for dense WDM (DWDM) scenarios in the C-band. The coupling region of each MRR is replaced by an MZI-based tunable coupler. Both the ring and the coupling region are integrated with a titanium micro-heater for independent thermal adjustment of the resonant wavelength and of the coupling coefficient. A pair of grating couplers are utilized to couple the optical signal in and out of this chip. The footprint of the dispersion compensator is 2 mm × 1 mm. See Methods for the detailed design, fabrication, and packaging of the Si<sub>3</sub>N<sub>4</sub> Kerr comb and of the dispersion compensator.

#### Characterizations of the dispersion compensator and data transmission using a CW laser

To achieve reconfiguration of the dispersion compensator for varying lengths of SMF, we devised an optimization algorithm that combines the transfer matrix method with the sequential quadratic programming (SQP) algorithm. This algorithm allowed us to determine the target parameters for the MRR-based dispersion compensator. We successfully demonstrated dispersion compensation for

SMF transmission up to 40 km within a bandwidth of 32 GHz. See Supplementary Note 2 for a detailed description of the optimization methodology and of the obtained results. Then, to facilitate an efficient dispersion compensation for diverse dispersion values, the optimized resonant wavelengths and coupling coefficients of all the MRRs for different dispersion conditions were documented in a look-up table. Accounting for the inherent fabrication deviations in silicon photonic devices, we deem it necessary the calibration of the random states for each MRR. Furthermore, we investigated the impact of thermal crosstalk on the tuning of the chip to their optimal configurations, considering the intra- and inter-thermal crosstalk within and between MRRs, respectively. By characterizing the tuning efficiencies influenced by the intra- and inter-thermal crosstalk and adjusting the applied voltages of MRRs correspondingly according to these efficiencies, we successfully compensated for the thermal crosstalk-induced resonant wavelength shifts.

Figures 2a and 2b show the measured transmission and group delay responses of dispersion compensation for a 40-km-long SMF with and without thermal crosstalk compensation (TCC). The implementation of TCC significantly alleviated these shifts, leading to a smoother and more linearly varied response within the operation bandwidth. For detailed information on the calibration process, see Supplementary Note 3. We note that the proposed TCC method is applicable to other photonic devices comprising multiple thermal phase shifters, which can significantly simplify the adjustment of the working states.

Figures 2c and 2e show the measured transmission spectra and the corresponding group delay responses covering a wavelength span from 1540 nm to 1580 nm after the calibration. The MRRs were calibrated at the wavelength of 1558.7 nm with a 32-GHz operation bandwidth for 10-km to 40-km SMFs. The enlarged views at the wavelength around 1558.7 nm are shown in Figs. 2d and 2f. The transmission spectra include the coupling loss of the grating couplers. The grating coupler has a maximum loss non-uniformity of ~3.5 dB over the 40 nm wavelength, which can be improved by using an edge coupler. The increased on-resonance transmission loss at the shorter wavelength side is due to the wavelength-dependent loss and the coupling coefficient of the MRRs. Figures 2g and 2h show the extracted insertion loss and the averaged dispersion of the dispersion compensator. The insertion loss is obtained at the center of the operation bandwidth of each channel, and the averaged dispersion is calculated as  $D_{avg} = (\tau_1 - \tau_2)/(\lambda_1 - \lambda_2)$ , where  $\lambda_1$  and  $\lambda_2$  are the shorter and longer wavelength ends across the operation bandwidth of each channel,  $\tau_1$  and  $\tau_2$  are the corresponding group delays, respectively. The insertion loss increases from ~8.4 dB to ~14.8 dB at the wavelength around 1558.7 nm for dispersion compensation of 10-km to 40-km SMFs, respectively. We can reduce the insertion loss by lowering the transmission loss of the silicon MRR waveguides. The averaged dispersion is -169.5 ps/nm, -325.4 ps/nm, -506.6 ps/nm, and -682.9 ps/nm for dispersion compensation of 10-km-, 20-km-, 30-km-, and 40-km-long SMFs at the same wavelength. The group delay increases slightly with the wavelength, which we attribute to the coupling coefficient variations of MRRs across wavelengths. The group delay degradation around 1540 nm is limited by the dynamic range of our measurement equipment, the Photonic Dispersion and Loss Analyzer (PDLA, Agilent 86038B).

Next, we conducted a 64 Gbit/s PAM4 signal transmission experiment using a continuous-wave (CW) laser as the light source to demonstrate the reconfigurability and the wide-band signal processing capability of our dispersion compensator in a wide wavelength span. We utilized an offline digital signal processing (DSP) algorithm with a time-domain feed-forward equalization (FFE) to recover the received signal. We note that no dispersion compensation algorithm was used in the

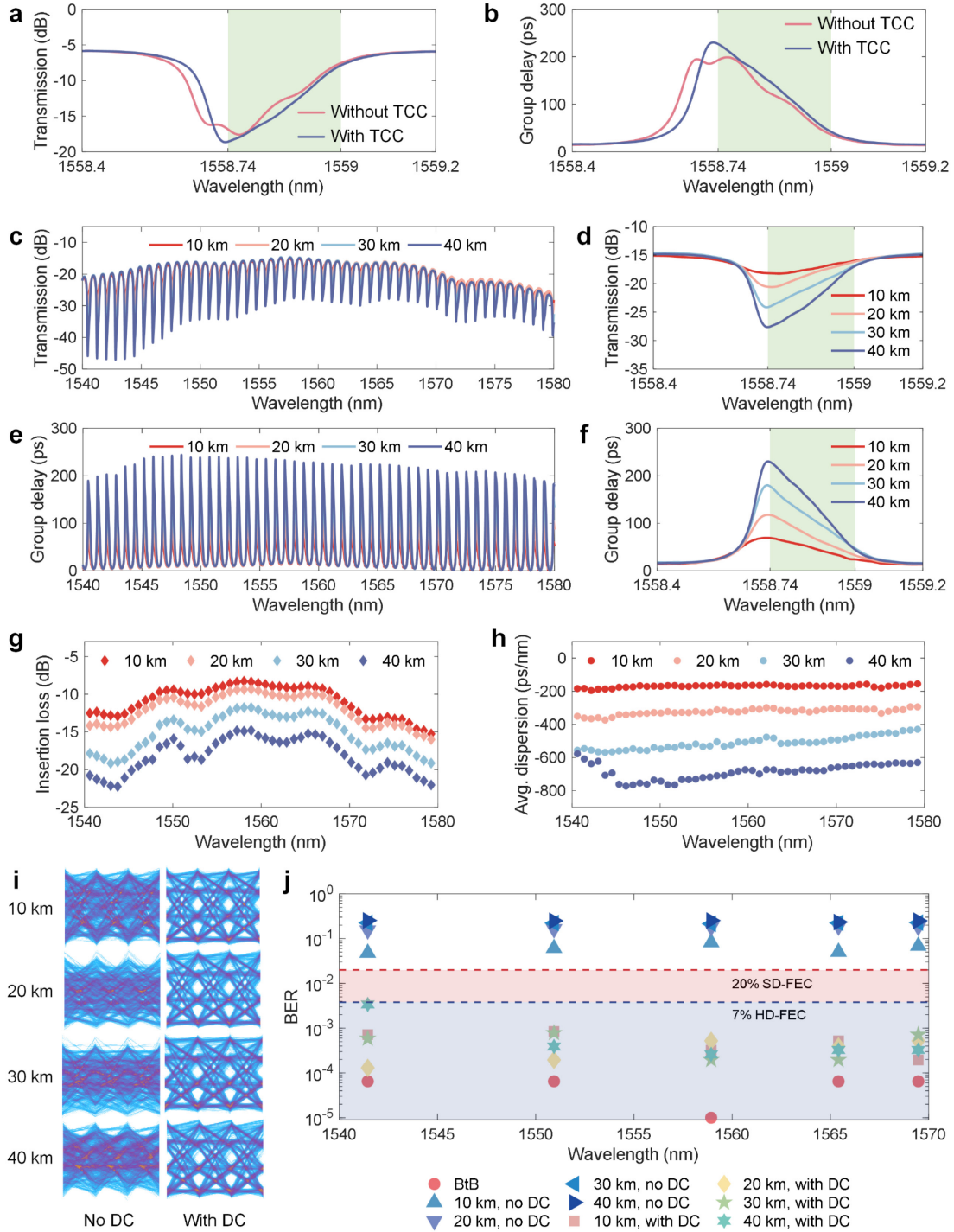


**Fig. 2. Characterizations of the dispersion compensator and data transmission using a CW-laser.** **a, b** Measured **(a)** transmission and **(b)** group delay responses with and without thermal crosstalk compensation for the dispersion compensation of 40-km-long SMF. TCC: thermal crosstalk compensation. **c** Measured transmission spectra for dispersion compensation of 10-km-, 20-km-, 30-km-, and 40-km-long SMFs in the wavelength range of 1540 nm to 1580 nm. **d** Enlarged view of the transmission spectra at the wavelength around 1558.7 nm. The operation bandwidth is calibrated to 32 GHz. **e** Measured group delay responses in the 40-nm wavelength span. **f** Enlarged view of the group delay responses at the wavelength of about 1558.7 nm. **g** Extracted insertion loss of each channel for dispersion compensation of different lengths of SMFs. The insertion loss is obtained at the center of the operation bandwidth. **h** Averaged dispersion of each channel for the 4 kinds

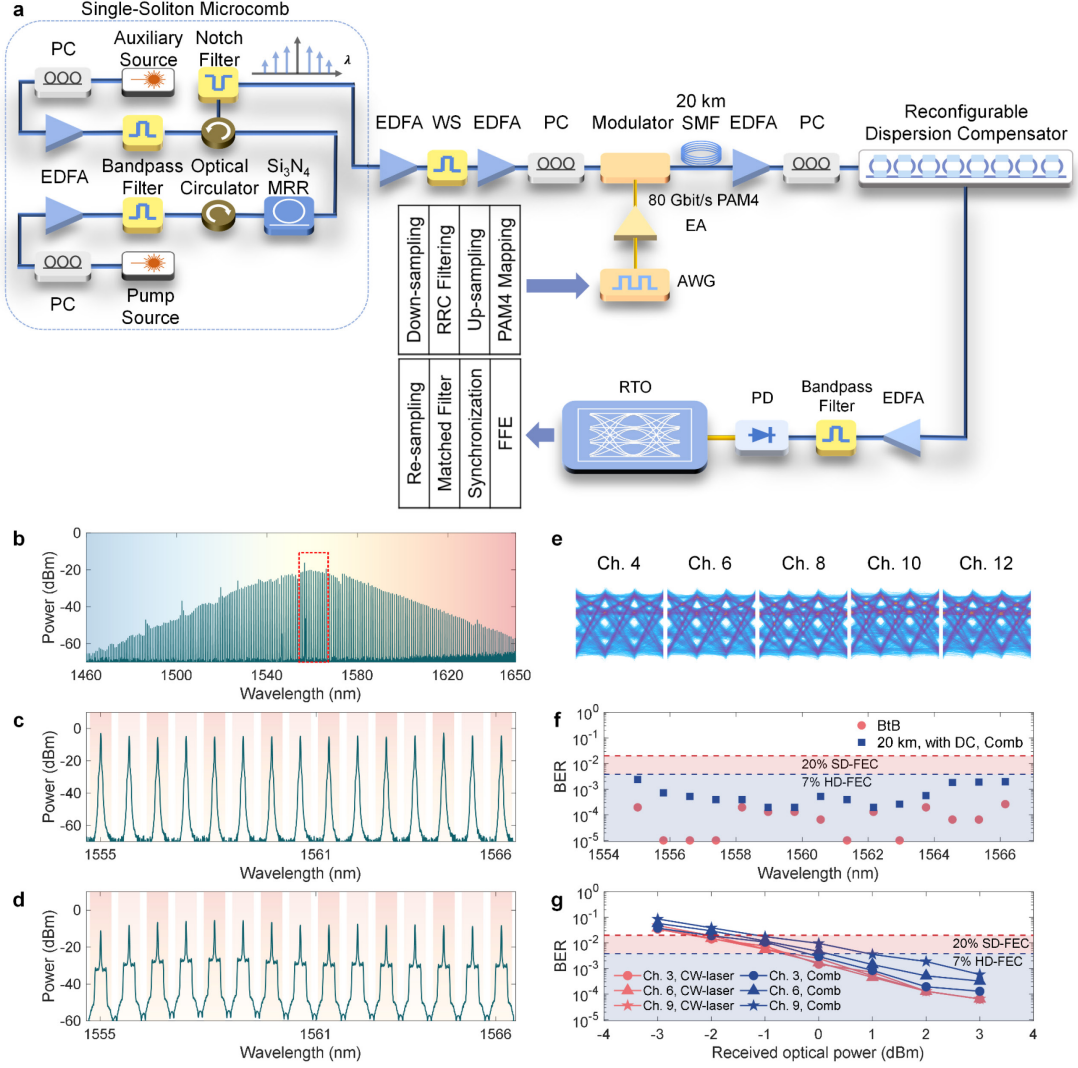
of dispersion compensation. **i** Measured PAM4 eye diagrams for the data transmission using a CW-laser as the light source at the wavelength of around 1558.96 nm for the four lengths of SMFs with and without dispersion compensation. 64-Gbit/s PAM4 signal is transmitted through SMFs. DC: dispersion compensation. **j** Measured BERs for data transmission under BtB transmission and SMFs transmissions with and without dispersion compensation at 5 different wavelengths in the 30-nm wavelength span ranging from 1540 nm to 1570 nm. BERs are much higher than the 20% SD-FEC threshold ( $2 \times 10^{-2}$ ) without the dispersion compensation, while they are all within the 7% HD-FEC threshold ( $3.8 \times 10^{-3}$ ) after the dispersion compensation.

signal receiving end. See Supplementary Note 4 for the detailed experimental setup. We measured 5 different wavelengths distributed from 1540 nm to 1570 nm under the 10-, 20-, 30-, and 40-km-long SMFs with and without dispersion compensation. The wavelength span was limited by our tunable bandpass filter. Figure 2i shows the measured eye diagrams for the transmissions with and without dispersion compensation at the wavelength of 1558.96 nm under the four lengths of SMFs. In the absence of dispersion compensation, the eye diagrams exhibit significant blurring. In contrast, with our dispersion compensator, the eye diagrams are successfully restored. The rest of the measured eye diagrams at the other wavelengths are included in Supplementary Note 4. The bit-error ratios (BERs) were also measured and shown in Fig. 2j. The BERs without dispersion compensator are all far beyond the 20% soft-decision forward-error correction (SD-FEC) threshold while all of them are below the 7% hard-decision forward-error correction (HD-FEC) threshold after dispersion compensation, demonstrating that our dispersion compensator exhibits a fairly good continuous dispersion compensation tunability and is capable of parallelly processing the data of at least 37 channels over the 30-nm wavelength range. The slightly higher BERs at wavelengths around 1540 nm and 1570 nm are due to the grating coupler-induced loss non-uniformity. The successful data transmission at the wavelength around 1540 nm indicates the degradation of the averaged dispersion of the 40-km-long SMF shown in Fig. 2h is limited by our instrument.

### **Parallel data transmission using a comb light source**

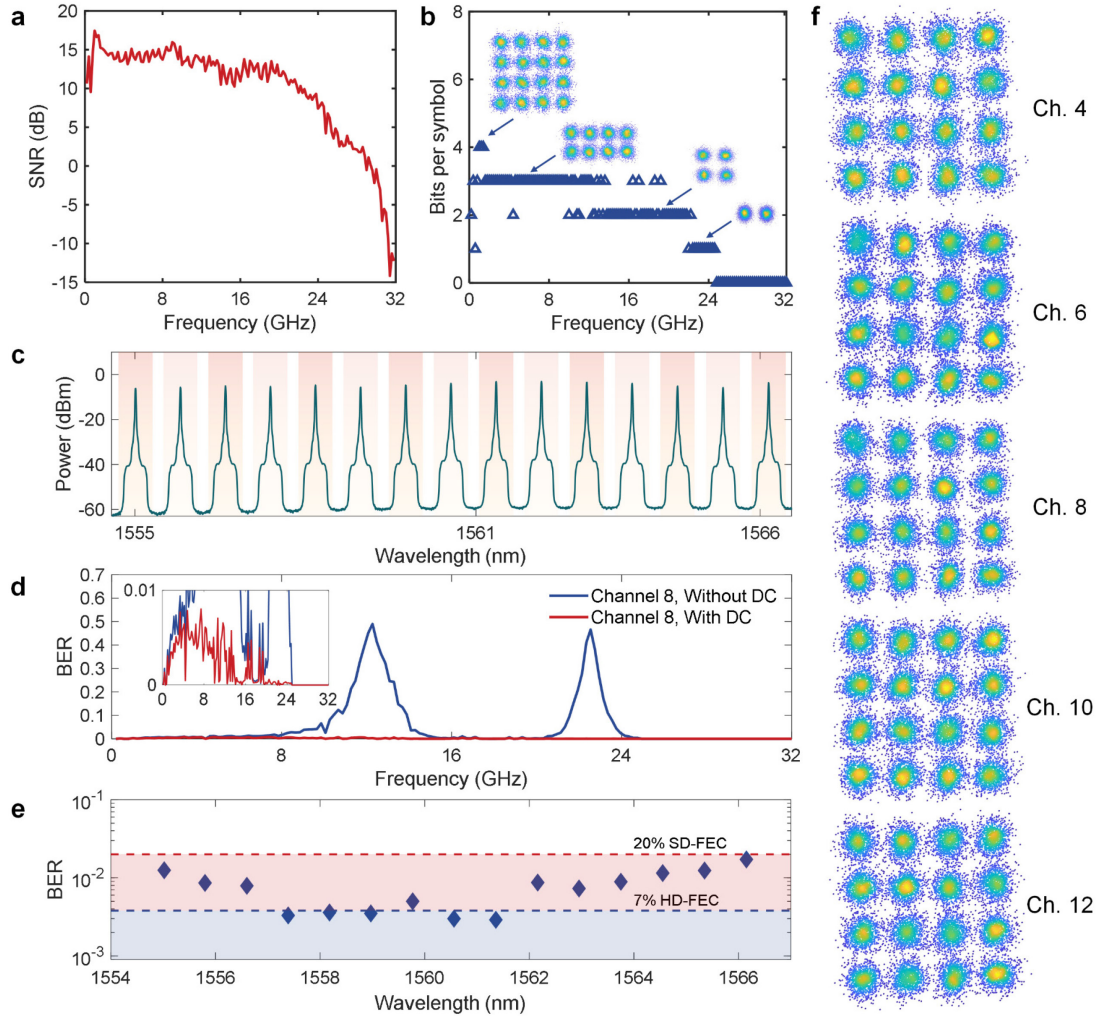
We demonstrated parallel data transmission and dispersion compensation using the  $\text{Si}_3\text{N}_4$  soliton comb lines as the light source. In this demonstration, we utilized a 20-km-long SMF in the transmission, and we calibrated our dispersion compensator for a 50-GHz operation bandwidth. See Supplementary Note 3 for the measured transmission spectra and group delay responses. The 80-Gbit/s PAM4 and 112-Gbit/s discrete multi-tone (DMT) signals were transmitted through the SMF, respectively.

Figure 3a shows the experimental setup of the PAM4 signal transmission. The spectrum of the generated single-soliton microcombs is depicted in Fig. 3b. The 10-dB spectral bandwidth of the single soliton is 62.6 nm, with 80 comb lines ranging from 1527 nm to 1590 nm included. Here the 10-dB spectral bandwidth describes the optical wavelength span of the spectrum with the optical power of the comb lines decreased by 10 dB from the comb line with the maximum power. As there is a slight FSR discrepancy between the comb lines ( $\sim 97.7$  GHz) and the dispersion compensators ( $\sim 99.5$  GHz), we only selected 15 comb lines from 1555 nm to 1563 nm by a programmable optical filter for the following data transmission. In principle, by carefully designing the FSRs of both devices with a smaller or even no discrepancy, we can select more wavelength channels for parallel data transmission. We utilized a single modulator to simultaneously modulate all the wavelength channels for simplicity. We detail the experimental settings and the DSP flows in Methods. The optical spectra of the reshaped and of the modulated comb lines are depicted in Figs. 3c and 3d, respectively.



**Fig. 3. 80-Gbit/s PAM4-based WDM data transmission with microcombs.** **a** Schematic experimental setup of a single-soliton microcomb driven parallel signal transmission system. PC: polarization controller; EDFA: erbium-doped fiber amplifier; WS: waveshaper; EA: electrical amplifier; AWG: arbitrary waveform generator; RTO: real-time oscilloscope; RRC: root-raised cosine; FFE: feed-forward equalization. **b** Measured spectrum of the generated single-soliton microcomb, which shows a  $\text{sech}^2$ -like spectral shape. The utilized 15 comb lines are indicated by a dashed box. **c** Measured spectrum of the chosen-out 15 comb lines after the waveshaper. **d** Measured spectrum of the 15 comb lines after the 40-Gbaud PAM4 modulation. **e** Measured eye diagrams of the 4<sup>th</sup>, 6<sup>th</sup>, 8<sup>th</sup>, 10<sup>th</sup>, and 12<sup>th</sup> channels after the dispersion compensation. **f** Measured BERs for the 15 WDM channels under the BtB transmission and the 20-km-long SMF transmission with dispersion compensation. All BERs are below the 7% HD-FEC threshold after dispersion compensation. DC: dispersion compensation. **g** BERs versus received optical power for the 20-km-long SMF transmissions of the 3<sup>rd</sup>, 6<sup>th</sup>, and 9<sup>th</sup> channels with dispersion compensation using the CW-laser and the microcomb as the light source, respectively.

Figure 3e shows the measured eye diagrams of the 4<sup>th</sup>, 6<sup>th</sup>, 8<sup>th</sup>, 10<sup>th</sup>, and 12<sup>th</sup> channels after transmission and dispersion compensation. See Supplementary Note 5 for the eye diagrams of all the 15 wavelength channels. All the 15 wavelength channels have good and comparable eye diagrams for the back-to-back (BtB) and for the 20-km-long SMF transmission. Figure 3f shows the measured BERs after dispersion compensation. Although a minor FSR difference between the comb lines and the channels of the dispersion compensator leads to a slightly higher BER level around the left and right



**Fig. 4. 112-Gbit/s DMT-based WDM transmission with microcombs.** **a** Measured signal-to-noise-ratio (SNR) response of the transmission system after the DMT training under the BtB transmission. **b** Bit allocations for DMT transmission within 32-GHz bandwidth. **c** Measured spectrum of the 15 comb lines after 112-Gbit/s DMT modulation. **d** Measured total BERs for the 8<sup>th</sup> channel with and without the dispersion compensation. Inset: The enlarged view of BER for transmission with dispersion compensation. DC: dispersion compensation. **e** BERs for WDM transmissions with dispersion compensation. All BERs are within the 20% SD-FEC threshold after dispersion compensation. **f** Measured 16-QAM constellations for the 4<sup>th</sup>, 6<sup>th</sup>, 8<sup>th</sup>, 10<sup>th</sup>, and 12<sup>th</sup> comb line channels at the 7<sup>th</sup> subcarrier.

sides of the wavelength span, all the BERs are below the 7% HD-FEC threshold, enabling a transmitted bit rate of 1.2 Tbit/s in total (1.12 Tbit/s net rate after FEC overhead subtraction). The BERs under different received optical powers for the CW-laser and the microcombs after dispersion compensation are illustrated in Fig. 3g. The 3<sup>rd</sup>, 6<sup>th</sup>, and 9<sup>th</sup> channels were chosen in the experiments, and the wavelengths of the CW-laser were kept the same as the ones of the selected comb lines. A trivial deterioration is observed between the BERs of the microcomb and the CW-laser transmission, demonstrating a comparable performance between these two light sources. The power penalty is ~1 dB at the 7% HD-FEC threshold.

To facilitate the next-generation data transmission rates, Common Electrical I/O (CEI)-112G standard based on 112 Gbit/s data rate transmission has been established by Optical Internetworking Forum (OIF)<sup>57</sup>. To achieve a 112 Gbit/s data rate per lane, we implemented the DMT

modulation format to increase the total data capacity. Compared with the PAM4 modulation format, DMT signals use a higher-order modulation format and can achieve a higher spectral efficiency for the microcomb-based WDM transmission system. The experimental setup of the DMT transmission is the same as that for the PAM4 transmission except that the DSP procedure is different, and the sampling rate of the arbitrary waveform generator (AWG) is set to be 64 GSa/s because of the limitation of the maximum length of the data sequence. The bandwidth of the dispersion compensator is still 50 GHz, and the DMT signal was mapped to a 32-GHz bandwidth with 160 sub-carriers. The details of the experimental setup are discussed in Methods. Before the data transmission, training of the DMT is essential to obtain the bit allocation of each tone. The training was carried out at the 9<sup>th</sup> channel under the BtB condition. The signal-to-noise-ratio (SNR) response and the bit allocation were obtained, which are shown in Figs. 4a and 4b. The maximum bit allocation is 4, corresponding to the modulation format of 16 quadratic amplitude modulation (16-QAM). Each sub-carrier was modulated with its own allocated modulation format. Then, we applied the identical bit allocation to all the 15 comb lines to ensure a uniform DMT setting.

Figure 4c illustrates the spectrum of the 112-Gbit/s DMT-modulated comb lines. Figure 4f depicts the measured 16-QAM constellations of the 7<sup>th</sup> sub-carrier for the 4<sup>th</sup>, 6<sup>th</sup>, 8<sup>th</sup>, 10<sup>th</sup>, and 12<sup>th</sup> channels. See Supplementary Note 6 for the constellations of all the 15 comb lines. Figure 4d shows the measured BERs for the 8<sup>th</sup> channel with and without dispersion compensation. The inset illustrates the enlarged view of the BER for transmission with dispersion compensation. At the frequency around 13 GHz and 23 GHz, the BERs reach as high as 0.49 and 0.47 before the dispersion compensation, respectively. We attribute this to the FSF of the 20-km SMF. See Supplementary Note 6 for the measured  $S_{21}$  response of the 20-km SMF. The BERs can be suppressed below 0.01 after dispersion compensation. The BERs of all the 15 channels after dispersion compensation are all below the 20% SD-FEC threshold, as shown in Fig. 4e. No FFE was introduced in the DMT transmission. In this case, an aggregate data rate of 1.68 Tbit/s (1.46 Tbit/s net rate) was achieved. The maximum power consumption of our dispersion compensator is as low as 160 mW. See Supplementary Note 6 for the detailed calculation of the bit rate and Supplementary Note 3 for the power consumption.

## Discussion

To our knowledge, we present the first demonstration of on-chip parallel signal transmission and dispersion compensation using a single-soliton microcomb and a dispersion compensator based on MRRs. Our optical dispersion compensator outperforms electronic dispersion compensation approaches based on DSP algorithms, which necessitate individual processing for each wavelength channel. In contrast, our optical dispersion compensator supports parallel dispersion compensation capabilities, irrespective of the modulation format and of the number of transmission channels. Compared with the dispersion compensators enabled by Bragg gratings and cascaded MZIs, the MRR-based dispersion compensator features a compact footprint and a flexible tuning capability. Notably, we achieved this parallel dispersion compensation with a low power consumption below 160 mW, underscoring its energy-efficient nature.

Furthermore, under the assumption of a matched FSR between the microcomb and the dispersion compensator, we can in principle utilize up to 51 channels from the microcomb for data transmission, which encompasses a wavelength span ranging from 1540 nm to 1580 nm. To achieve a total bit rate exceeding 10 Tbit/s, the spacing between adjacent comb lines can be further reduced to 50 GHz. It is worth noting that we can integrate various components such as a Si<sub>3</sub>N<sub>4</sub> microcomb,

a silicon MRR-based dispersion compensator, MRR modulators, photodetectors, and optical de-/multiplexers onto a single chip. By accomplishing this, we can realize a fully integrated optical communications system tailored specifically for short-reach DCIs.

In the experiment, the single-soliton microcomb in the microresonator with anomalous dispersion demonstrates a conversion energy efficiency of approximately 1%. The power of most of the comb lines is below -20 dBm (considering the coupling and link loss). Investigations highlighting the effectiveness of utilizing a double-microring structure have been proposed with a high conversion energy efficiency of 55% for single soliton generation<sup>58</sup>, resulting in increased power levels for the majority of the comb lines to -10 dBm, which reduces the gain required by the erbium-doped fiber amplifier (EDFA). Consequently, this leads to improved noise characteristics and facilitates higher bit rates for each carrier. To further enhance the overall performance of the system, it is plausible to minimize the fiber-to-fiber loss associated with the dispersion compensator by introducing low-loss and broadband edge couplers<sup>59-61</sup>. Additionally, MRRs made of widened waveguides can be incorporated to mitigate on-chip losses. By implementing these strategies, we believe a higher number of microcomb channels can be effectively utilized for data transmission.

## Conclusion

We have presented parallel data transmission and dispersion compensation utilizing a Si<sub>3</sub>N<sub>4</sub> single-soliton microcomb and a silicon MRR-based dispersion compensator. With the full reconfigurability of the MRRs, our dispersion compensator achieves a continuously tunable dispersion compensation of up to 40 km SMFs within a 32-GHz bandwidth, and a dispersion compensation of 20-km-long SMF within a 50-GHz bandwidth. We proposed a method for calibration of the MRR-based dispersion compensator, which can eliminate the thermal crosstalk and is applicable to other integrated photonic circuits. Our experimentation with the Si<sub>3</sub>N<sub>4</sub> single-soliton microcomb revealed the utilization of 15 comb lines for parallel data transmission, resulting in an aggregate total bit rate of 1.2 Tbit/s and of 1.68 Tbit/s using 80-Gbit/s PAM4 and 112-Gbit/s DMT modulation signals for 20-km SMF transmission, respectively. These demonstrations in utilizing the microcomb and the silicon photonic circuits enable a higher data transmission capacity, potentially lower costs, and power-efficient solutions for parallel data processing, especially in WDM-assisted IM-DD systems. Our findings represent a significant advancement toward the pragmatic applications of cost-effective and practical short-reach DCIs.

## Methods

### Design, fabrication, and packaging of the silicon photonic dispersion compensator chip

The coupling region of each microring comprises an MZI-based tunable coupler, which comprises two 50:50 multimode interferometers (MMIs), two 165- $\mu$ m-long straight arms, and waveguide connections between them. The feedback region of each microring comprises a 335- $\mu$ m-long straight waveguide and two 10- $\mu$ m-radius arc bends. The dimensions of the waveguide cross-section are 500 nm (width)  $\times$  220 nm (height). Two 160- $\mu$ m-long and 2- $\mu$ m-wide titanium micro-heaters, with a resistance of about 1800  $\Omega$ , are integrated 2- $\mu$ m above the center of the 335- $\mu$ m-long straight waveguide and of the lower arm of the MZI coupler. Deep trenches are positioned beside each micro-heater to suppress the thermal crosstalk within the MRR.

The device was fabricated on a silicon-on-insulator (SOI) platform with a 220-nm-thick silicon top layer and a 2- $\mu$ m buried oxide (BOX) using electron-beam lithography. All the devices except for

the grating couplers were fully etched to a depth of 220 nm. A 70-nm partial etch was implemented on the grating coupler regions. The gold metal connections were deposited above the titanium micro-heaters for electrical contacts. The metal pads were wire-bonded to an external printed-circuit board (PCB). The chip and the PCB were placed on a metal shell, and a thermo-electric cooler (TEC) was placed beneath the chip to control the on-chip temperature.

#### **Design, fabrication, and packaging of the Si<sub>3</sub>N<sub>4</sub> microcomb chip**

The Si<sub>3</sub>N<sub>4</sub> microresonator has waveguide cross-sectional dimensions of 1800 nm (width) × 800 nm (height), with the fundamental TE mode exhibiting anomalous dispersion. The radius of the microresonator is 232 μm, resulting in an FSR of 97.7 GHz. The ultra-low-loss waveguide was fabricated on an 800-nm-thick Si<sub>3</sub>N<sub>4</sub> layer, deposited by low-pressure chemical vapor deposition (LPCVD) by Ligentec. The device was patterned using 193-nm photolithography and the quality (Q) factor of the microring resonator is  $7 \times 10^5$  to support the generation of the soliton microcomb. The Si<sub>3</sub>N<sub>4</sub> chip was packaged with a pair of fiber arrays and the coupling loss is ~3 dB/facet after being fixed by an ultra-violet (UV) curable adhesive. We utilized a TEC to control the on-chip temperature for the long-term single-soliton generation.

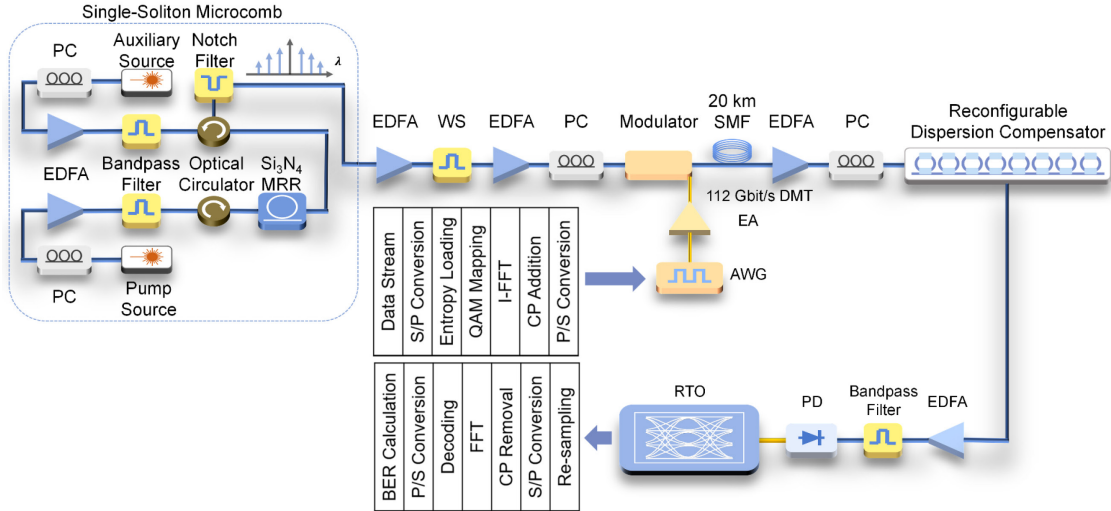
#### **Experimental settings and DSP flows of PAM4 parallel data transmission**

For the 80-Gbit/s PAM4-based parallel data transmission, the generated comb lines were first amplified to a total power of 20 dBm, and then they were sent into a programmable optical filter (Finisar Waveshaper 1000S) to select 15 comb lines and to ensure that the power of each comb line was almost identical to each other. Then, another EDFA was utilized to amplify the 15 comb lines to a total power of 17.5 dBm. Next, the optical comb lines were simultaneously modulated by a commercial 40-GHz intensity modulator (iXblue MXAN-LN-40) driven by an PAM4 signal generated from an AWG (Keysight 8199A). The modulated comb lines were sent into the 20-km SMF, and the dispersion was then compensated for by our dispersion compensator. Then, one channel of the dispersion-compensated parallel signals was filtered out by a tunable narrow-bandwidth optical filter and was directly detected by a commercial 50-GHz photodetector (Finisar XPDV2320R). The received electrical signal was finally recorded by a real-time oscilloscope (RTO, Keysight Z592A), and a DSP algorithm, which is identical to the one utilized in the CW-laser transmission, was applied to process offline the received data. At the transmitter side, a high-speed PAM4 signal was transmitted using the root-raised cosine (RRC) filter with a roll-off factor of 0.01 to compress the signal bandwidth. The matched filter and the time-domain FFE were applied at the receiver side to obtain lower BERs. The instruments and their settings were consistent with those in the CW-laser transmission. The optical power before the photodetector was set to the same power to ensure consistency.

#### **Experimental setup and DSP flows of DMT parallel data transmission**

Extended Data Figure 1 shows the schematic experimental setup of the microcomb-based data transmission using the DMT modulation format. A high-speed pseudo-random binary sequence (PRBS) data stream was divided into several parallel low-speed data streams and was mapped to a QAM constellation map. The complex values corresponding to each point in the constellation map were converted to real numbers by an inverse fast Fourier transform (I-FFT). A total number of 160 sub-carriers was mapped to the 32-GHz frequency range. Finally, the signals were converted to a serial data stream after adding the cyclic prefix (CP) to compensate for the multipath delay

418 broadening. At the receiver side, the photocurrent signal was sent to the RTO for data collection.  
 419 The CP was first removed from the sampled data sequence. Next, the serial data was converted to  
 420 parallel data and mapped to the QAM constellation map through a fast Fourier transform (FFT). The  
 421 BERs of the full link were then calculated by comparing the measured data sequence with the  
 422 transmitter data sequence.



423  
 424 **Extended Data Fig. 1 Experimental setup of the DMT parallel data transmission.** P/S Conversion: parallel  
 425 to serial conversion; S/P Conversion: serial to parallel conversion; FFT: fast Fourier transform; I-FFT: inverse  
 426 fast Fourier transform; QAM: quadratic amplitude modulation; CP: cyclic prefix.

427 **Acknowledgements**

428 This work was supported in part by the National Key Research and Development Program of China  
 429 (2018YFB2201702), and the National Natural Science Foundation of China (62090052, 62135010,  
 430 62075128).

431 **Author contributions**

432 Y. Liu designed, simulated, and characterized the dispersion compensator. Y. Liu performed the  
 433 experiments of the CW-laser-based 64-Gbit/s PAM4 data transmission. H. Zhang designed,  
 434 simulated, and characterized the Kerr microcomb. Y. Liu and H. Zhang conceived the link  
 435 architecture and performed the high-speed data-transmission experiments of the microcomb-based  
 436 parallel signal processing. J. Liu conducted the offline DSP. All authors helped analyze the data. L.  
 437 Lu, J. Du, Y. Liu, H. Zhang, and J. Liu prepared the manuscript.

438 **Conflict of interest**

439 The authors declare that they have no conflict of interest.

440 **References**

441 1. Forbes. 175 Zettabytes by 2025 <https://www.forbes.com/sites/tomcoughlin/2018/11/27/175-zettabytes-by-2025/>,  
 442 (2018).  
 443 2. Chopra R. Looking beyond 400G - A system vendor perspective. Cisco Systems Inc  
 444 [https://www.ethernalliance.org/wp-content/uploads/2021/02/TEF21Day1\\_KeynoteRChoprapdf](https://www.ethernalliance.org/wp-content/uploads/2021/02/TEF21Day1_KeynoteRChoprapdf), (2020).  
 445 3. Pang XD, *et al.* 200 Gbps/Lane IM/DD Technologies for Short Reach Optical Interconnects. *Journal of Lightwave*  
 446 *Technology* **38**, 492-503 (2020).

4. Alam MS, *et al.* Net 220 Gbps/ $\lambda$  IM/DD Transmssion in O-Band and C-Band With Silicon Photonic Traveling-Wave MZM. *Journal of Lightwave Technology* **39**, 4270-4278 (2021).
5. Zhang J, *et al.* Receive-diversity-aided power-fading compensation for C-band IM/DD OFDM systems. *Opt Lett* **48**, 2237-2240 (2023).
6. Zou D, Li F, Wang W, Li Z, Li Z. Amplifier-less transmission of beyond 100-Gbit/s/ $\lambda$  signal for 40-km DCI-Edge with 10G-class O-band DML. *Journal of Lightwave Technology* **38**, 5649-5655 (2020).
7. Wu X, Karar AS, Zhong K, Lau APT, Lu C. Experimental demonstration of pre-electronic dispersion compensation in IM/DD systems using an iterative algorithm. *Opt Express* **29**, 24735-24749 (2021).
8. Karar AS. Iterative Algorithm for Electronic Dispersion Compensation in IM/DD Systems. *Journal of Lightwave Technology* **38**, 698-704 (2020).
9. Zou DD, Li F, Wang W, Yin MZ, Sui Q, Li ZH. Modified Gerchberg-Saxton Algorithm Based Electrical Dispersion Pre-Compensation for Intensity-modulation and Direct-detection Systems. *Journal of Lightwave Technology* **40**, 2840-2849 (2022).
10. Zou DD, *et al.* 100G PAM-6 and PAM-8 Signal Transmission Enabled by Pre-Chirping for 10-km Intra-DCI Utilizing MZM in C-band. *Journal of Lightwave Technology* **38**, 3445-3453 (2020).
11. Yin M, Zou D, Wang W, Li F, Li Z. Transmission of a 56 Gbit/s PAM4 signal with low-resolution DAC and pre-equalization only over 80 km fiber in C-band IM/DD systems for optical interconnects. *Opt Lett* **46**, 5615-5618 (2021).
12. Zhong KP, Zhou X, Huo JH, Yu CY, Lu C, Lau APT. Digital Signal Processing for Short-Reach Optical Communications: A Review of Current Technologies and Future Trends. *Journal of Lightwave Technology* **36**, 377-400 (2018).
13. Wu X, Zhang J, Lau APT, Lu C. C-band 100-GBaud PS-PAM-4 transmission over 50-km SSMF enabled by FIR-filter-based pre-electronic dispersion compensation. *Opt Express* **31**, 17759-17768 (2023).
14. Kilper DC, Rastegarfar H. Energy challenges in optical access and aggregation networks. *Philosophical Transactions of the Royal Society A: Mathematical, Physical and Engineering Sciences* **374**, 20140435 (2016).
15. Yang KY, *et al.* Bridging ultrahigh-Q devices and photonic circuits. *Nature Photonics* **12**, 297-303 (2018).
16. Brasch V, *et al.* Photonic chip-based optical frequency comb using soliton Cherenkov radiation. *Science* **351**, 357-360 (2016).
17. Guo H, *et al.* Universal dynamics and deterministic switching of dissipative Kerr solitons in optical microresonators. *Nature Physics* **13**, 94-102 (2016).
18. Herr T, *et al.* Temporal solitons in optical microresonators. *Nature Photonics* **8**, 145-152 (2013).
19. Liu JQ, *et al.* Ultralow-power chip-based soliton microcombs for photonic integration. *Optica* **5**, 1347-1353 (2018).
20. Shen B, *et al.* Integrated turnkey soliton microcombs. *Nature* **582**, 365-369 (2020).
21. Stern B, Ji X, Okawachi Y, Gaeta AL, Lipson M. Battery-operated integrated frequency comb generator. *Nature* **562**, 401-405 (2018).
22. Yi X, Yang QF, Yang KY, Suh MG, Vahala K. Soliton frequency comb at microwave rates in a high-Q silica microresonator. *Optica* **2**, 1078-1085 (2015).
23. Zhang SY, *et al.* Sub-milliwatt-level microresonator solitons with extended access range using an auxiliary laser. *Optica* **6**, 206-212 (2019).
24. Zhou H, *et al.* Soliton bursts and deterministic dissipative Kerr soliton generation in auxiliary-assisted microcavities. *Light: Science & Application* **8**, 50 (2019).
25. Marin-Palomo P, *et al.* Microresonator-based solitons for massively parallel coherent optical communications. *Nature* **546**, 274-279 (2017).
26. Corcoran B, *et al.* Ultra-dense optical data transmission over standard fibre with a single chip source. *Nature*

- Communications* **11**, 2568 (2020).
27. Jørgensen AA, *et al.* Petabit-per-second data transmission using a chip-scale microcomb ring resonator source. *Nature Photonics* **16**, 798-802 (2022).
  28. Geng Y, *et al.* Coherent optical communications using coherence-cloned Kerr soliton microcombs. *Nature Communications* **13**, 1070 (2022).
  29. Mazur M, *et al.* High Spectral Efficiency Coherent Superchannel Transmission With Soliton Microcombs. *Journal of Lightwave Technology* **39**, 4367-4373 (2021).
  30. Fulop A, *et al.* High-order coherent communications using mode-locked dark-pulse Kerr combs from microresonators. *Nature Communications* **9**, 1598 (2018).
  31. Rizzo A, *et al.* Massively scalable Kerr comb-driven silicon photonic link. *Nature Photonics*, (2023).
  32. Shu H, *et al.* Microcomb-driven silicon photonic systems. *Nature* **605**, 457-463 (2022).
  33. Liu SJ, Zhang CP, Cao HY, Hong SH, Yu ZJ, Dai DX. On-Chip Circulator-Free Chirped Spiral Multimode Waveguide Grating for Dispersion Management. *ACS Photonics* **10**, 1654-1661 (2023).
  34. Kaushal S, Roberge A, Kashyap R, Azana J. Ultra-compact silicon photonics highly dispersive elements for low-latency signal processing. *Opt Express* **31**, 3467-3478 (2023).
  35. Chen GF, Ong KYK, Chia XX, Cao Y, Tan DTH. Dispersion Compensation of 30GBaud/s NRZ and PAM4 data using integrated Silicon Nitride Gratings. In: *Optical Fiber Communications Conference and Exhibition (OFC), paper Th1D.4* (2022).
  36. Liu SJ, Liu DJ, Yu ZJ, Liu L, Shi YC, Dai DX. Digitally tunable dispersion controller using chirped multimode waveguide gratings. *Optica* **10**, 316-323 (2023).
  37. Giuntori I, *et al.* Integrated Drop-Filter for Dispersion Compensation Based on SOI Rib Waveguides. *Conference on Optical Fiber Communication and Collocated National Fiber Optic Engineers Conference (OFC-NFOEC), paper OThj5*, (2010).
  38. Moreira R, Gundavarapu S, Blumenthal DJ. Programmable eye-opener lattice filter for multi-channel dispersion compensation using an integrated compact low-loss silicon nitride platform. *Opt Express* **24**, 16732-16742 (2016).
  39. Brodnik GM, Pinho C, Chang F, Blumenthal DJ. Extended Reach 40km Transmission of C-Band Real-Time 53.125 Gbps PAM-4 Enabled with a Photonic Integrated Tunable Lattice Filter Dispersion Compensator. In: *Optical Fiber Communications Conference and Exposition (OFC), paper W2A.30* (2018).
  40. Madsen CK, *et al.* An All-Pass Filter Dispersion Compensator Using Planar Waveguide Ring Resonators. In: *Optical Fiber Communication Conference and the International Conference on Integrated Optics and Optical Fiber Communication, paper FE6* (1999).
  41. Madsen CK, Lenz G, Bruce AJ, Cappuzzo MA, Gomez LT, Scotti RE. Integrated all-pass filters for tunable dispersion and dispersion slope compensation. *IEEE Photonics Technology Letters* **11**, 1623-1625 (1999).
  42. Notaros J, *et al.* Programmable dispersion on a photonic integrated circuit for classical and quantum applications. *Opt Express* **25**, 21275-21285 (2017).
  43. Sorianoello V, *et al.* 100Gb/s PolMux-NRZ Transmission at 1550nm over 30km Single Mode Fiber Enabled by a Silicon Photonics Optical Dispersion Compensator. In: *Optical Fiber Communication Conference (OFC), paper W2A.31* (2018).
  44. Alam MS, *et al.* 224 Gb/s Transmission over 10 km of SMF at 1550 nm Enabled by a SiN Optical Dispersion Compensator and Stokes Vector Direct Detect Receiver. In: *OSA Advanced Photonics Congress (APC), paper SpM4I.5* (2020).
  45. Liu Y, Lu L, Ni Z, Chen J, Chen J, Zhou L. Silicon Integrated Continuously Tunable Dispersion Compensator Based on Cascaded Micro-Ring Resonators. In: *2022 Asia Communications and Photonics Conference (ACP)* (2022).
  46. Ong KYK, Chen GFR, Xing P, Gao H, Tan DTH. Dispersion compensation of high-speed data using an integrated

- p>silicon nitride ring resonator.
- Opt Express*
- 30**
- , 13959-13967 (2022).
47. Zhang Y, *et al.* 240 Gb/s optical transmission based on an ultrafast silicon microring modulator. *Photon Res* **10**, 1127-1133 (2022).
  48. Dong P. Silicon Photonic Integrated Circuits for Wavelength-Division Multiplexing Applications. *IEEE Journal of Selected Topics in Quantum Electronics* **22**, 370-378 (2016).
  49. Liu D, Zhang L, Tan Y, Dai D. High-Order Adiabatic Elliptical-Microring Filter with an Ultra-Large Free-Spectral-Range. *Journal of Lightwave Technology* **39**, 5910-5916 (2021).
  50. Liu DJ, He JH, Xiang YL, Xu Y, Dai DX. High-performance silicon photonic filters based on all-passive tenth-order adiabatic elliptical-microrings. *Appl Photonics* **7**, 051303 (2022).
  51. Horst F, Green WMJ, Assefa S, Shank SM, Vlasov YA, Offrein BJ. Cascaded Mach-Zehnder wavelength filters in silicon photonics for low loss and flat pass-band WDM (de-)multiplexing. *Opt Express* **21**, 11652-11658 (2013).
  52. Jeong SH, Shimura D, Simoyama T, Horikawa T, Tanaka Y, Morito K. Si-nanowire-based multistage delayed Mach-Zehnder interferometer optical MUX/DeMUX fabricated by an ArF-immersion lithography process on a 300 mm SOI wafer. *Opt Lett* **39**, 3702-3705 (2014).
  53. Sun Q, Zhou L, Lu L, Zhou G, Chen J. Reconfigurable High-Resolution Microwave Photonic Filter Based on Dual-Ring-Assisted MZIs on the Si<sub>3</sub>N<sub>4</sub> Platform. *IEEE Photonics Journal* **10**, 1-12 (2018).
  54. Kohli N, Sang BL, Nabki F, Ménard M. Tunable Bandpass Filter With Serially Coupled Ring Resonators Assisted MZI. *IEEE Photonics Journal* **13**, 1-8 (2021).
  55. Fujii S, Tanabe T. Dispersion engineering and measurement of whispering gallery mode microresonator for Kerr frequency comb generation. *Nanophotonics* **9**, 1087-1104 (2020).
  56. Zhang HY, Lu LJ, Chen JP, Zhou LJ. Program-Controlled Single Soliton Generation Driven by the Thermal-Compensated Avoided Mode Crossing. *Journal of Lightwave Technology* **41**, 1801-1810 (2023).
  57. OIF. Common Electrical I/O (CEI) -Electrical and Jitter Interoperability agreements for 6G+ bps, 11G+ bps, 25G+ bps, 56G+ bps and 112G+ bps I/O. (2022).
  58. Helgason óB, Girardi M, Ye Z, Lei F, Schröder J, Torres-Company V. Power-efficient soliton microcombs. *arXiv:202209410*, (2022).
  59. He A, Guo X, Wang K, Zhang Y, Su Y. Low Loss, Large Bandwidth Fiber-Chip Edge Couplers Based on Silicon-on-Insulator Platform. *Journal of Lightwave Technology* **38**, 4780-4786 (2020).
  60. Liu W, Zhang J, Liu L, Dai D, Shi Y. High Efficiency Silicon Edge Coupler Based On Uniform Arrayed Waveguides With Un-Patterned Cladding. *IEEE Photonics Technology Letters* **32**, 1077-1080 (2020).
  61. Marchetti R, Lacava C, Carroll L, Gradkowski K, Minzioni P. Coupling strategies for silicon photonics integrated chips [Invited]. *Photon Res* **7**, 201-239 (2019).

## Supplementary Files

This is a list of supplementary files associated with this preprint. Click to download.

- [SupplementaryInformation.pdf](#)